

Analogue Quantum Simulation with Fixed-Frequency Transmon Qubits

Sean Greenaway,¹ Adam Smith,^{2,3} Florian Mintert,^{1,4} and Daniel Malz^{5,6}

¹*Physics Department, Blackett Laboratory, Imperial College London,
Prince Consort Road, SW7 2BW, United Kingdom*

²*School of Physics and Astronomy, University of Nottingham, Nottingham, NG7 2RD, UK*

³*Centre for the Mathematics and Theoretical Physics of Quantum Non-Equilibrium Systems,
University of Nottingham, Nottingham, NG7 2RD, UK*

⁴*Helmholtz-Zentrum Dresden-Rossendorf, Bautzner Landstraße 400, 01328 Dresden, Germany*

⁵*Max-Planck-Institute of Quantum Optics, Hans-Kopfermann-Str. 1, 85748 Garching, Germany*

⁶*Department of Physics, Technische Universität München,
James-Frank-Straße 1, 85748 Garching, Germany*

(Dated: November 30, 2022)

We experimentally assess the suitability of transmon qubits with fixed frequencies and fixed interactions for the realization of analogue quantum simulations of spin systems. We test a set of necessary criteria for this goal on a commercial quantum processor using full quantum process tomography and more efficient Hamiltonian tomography. Significant single qubit errors at low amplitudes are identified as a limiting factor preventing the realization of analogue simulations on currently available devices. We additionally find spurious dynamics in the absence of drive pulses, which we identify with coherent coupling between the qubit and a low dimensional environment. With moderate improvements, analogue simulation of a rich family of time-dependent many-body spin Hamiltonians may be possible.

I. INTRODUCTION

Recent experimental progress towards the development of fault-tolerant quantum computers has been considerable [1]. However, the current so-called *noisy intermediate scale quantum* (NISQ) devices are limited by a level of noise that at present precludes implementation of many algorithms [2]. An exciting application which is thought to be achievable even in the presence of noise, lies in the quantum simulation of physical systems for which classical simulations are intractable [3].

A wide array of experimental platforms have already demonstrated many of the commonly-applied criteria [4] for the realization of quantum simulations [5–8]. The digital approach towards implementing such a simulation typically involves decomposing the time evolution operator into a series of implementable gates through Trotterization [9], an approach that has been demonstrated for a variety of small systems experimentally on NISQ devices [10–12]. Such gate-based quantum simulations are highly flexible, being capable (in principle at least) of simulating any quantum system due to the universality of quantum computation. In practise, these simulations are restricted to small system sizes and short simulation times, since increasing either necessitates more gates, which come with a commensurate increase in error.

An alternative approach, known as *analogue quantum simulation* [3] directly simulates a system of interest by manipulating a controllable experimental system that mimics it, allowing for decomposition protocols such as Trotterization to be circumvented. The increased efficiency of analogue simulation has allowed for the simulation of larger quantum systems for longer times than gate-based approached in platforms such as cold

atoms [13–15] and has motivated substantial research into implementations in other platforms such as superconducting circuits [16–19]. This efficiency comes at the expense of limiting the simulations to the system’s “native” Hamiltonians. Additionally, such analogue simulators may be restricted in the measurements that can be performed upon them, in contrast to gate-based devices which have access to general Pauli string measurements. This motivates the search for alternative quantum simulation platforms to complement the existing ones.

In order to implement an analogue quantum simulation, it is crucial that the map between an applied control protocol and the resulting experimental effective Hamiltonian is well understood. To this end three criteria may be identified that are necessary for the experimental implementation of analogue quantum simulations [4, 20]:

- (C1) *Expressibility*: The experimental Hamiltonian must permit control protocols which allow for some class (or multiple classes) of interesting models to be simulated.
- (C2) *Controllability*: It should be possible to switch individual control terms on and off independently, without inducing significant errors on other qubits.
- (C3) *Stability*: The map between the control protocol and the experimental effective Hamiltonian should be stable enough over time that characterization and simulation experiments can be performed without the map changing due to, for example, parameter drift. Additionally, the coherence time of the device should be sufficiently long to allow simulations to be performed.

In this work we experimentally assess the extent to which fixed-frequency, fixed-interaction (FF) transmon qubits

available through the IBM Quantum cloud-based platform [21] satisfy these criteria, and thereby probe the utility of this system as a platform for analogue quantum simulation. As a platform primarily used for gate-based quantum computation, FF transmon qubits allow for the control of individual qubits and arbitrary Pauli string measurements [22]. Additionally, the underlying physical Hamiltonian used to implement these gates may be mapped to a wide array of interesting Hamiltonians which may be simulated [23]. As such, FF transmon devices are potentially highly useful as a platform for analogue simulation.

FF transmon devices can be modelled as weakly coupled Duffing oscillators controlled via time-dependent drive pulses. Two-body entanglement can be generated through a cross-resonance interaction, in which a qubit is driven at the resonant frequency of another to which it is coupled [24, 25]. This procedure results in an entangling operation comprised of ZX and ZY terms (where $\mathbb{1}, X, Y, Z$ are the Pauli matrices and the tensor product is implied) along with a number of spurious single qubit terms. In order to use this platform for analogue quantum simulation, the magnitude of these terms must be well known such that they can be controlled during a simulation. If this can be achieved, FF transmon qubits should allow for a rich class of systems to be simulated, including Ising Hamiltonians with individually addressable Ising coupling and single qubit magnetic field control, systems with XY -type interactions and the quantum East model [26]. Thus, they satisfy criterion (C1).

While the effective Hamiltonian resulting from applying cross-resonance drives can be derived rigorously using Floquet theory [27], the resulting predictions are not sufficiently precise to run high-fidelity simulations. Instead, we characterize the device experimentally. First, we use full quantum process tomography (QPT) to show that it is possible to individually and independently control the cross-resonance interaction, and to find the dominant spurious terms. Second, we use Hamiltonian tomography to accurately and efficiently extract the Hamiltonian rates.

We characterize the unwanted single-qubit terms generated through the cross-resonance drives and extract phase, amplitude and detuning errors. In principle, these can be cancelled using weak additional tones, but we observe that the drive amplitudes cannot be controlled with sufficient precision to do so, which could be fixed with hardware improvements.

Additionally, we identify spurious dynamics in the absence of driving with coupling between two level system (TLS) defects and the transmon qubits. The error terms arising from these fluctuate significantly over time, meaning that the IBM Quantum devices do not satisfy criterion (C3). This, rather than imperfections with the entangling operation, is identified as the key limiting factor preventing the realization of fully-controllable analogue quantum simulations on current-generation FF transmon devices.

II. CONTROLLING FIXED-FREQUENCY, FIXED-INTERACTION TRANSMON QUBITS

The starting point for the analysis presented here is the verification of the model used to inform experimental control protocols. For FF transmon qubits, the system can be described as a series of n coupled Duffing oscillators, for which the Hamiltonian is [22, 23]

$$H^{\text{duff}} = \sum_{i=1}^n \left(\omega_i a_i^\dagger a_i + \alpha_i a_i^\dagger a_i^\dagger a_i a_i + D_i(t)(a_i + a_i^\dagger) \right) + \sum_{\langle i,j \rangle} J_{ij}(a_i - a_i^\dagger)(a_j - a_j^\dagger), \quad (1)$$

where ω_i and α are the harmonic frequency and anharmonicity of the i th transmon respectively, J_{ij} is the capacitive coupling strength between the i th and j th transmon, where the nearest-neighbour notation $\langle i, j \rangle$ reflects the physical connectivity of the device, and the drive on the i th transmon is given by

$$D_i(t) = \frac{\Omega}{2} \text{Re} \left[e^{i(\omega_i + \Delta_i)t} d_i(t) \right], \quad (2)$$

with drive strength Ω , applied detuning Δ_i and dimensionless drive envelope $d(t)$. For high enough anharmonicities relative to the applied drive strength, the transition between the states $|0\rangle$ and $|1\rangle$ is well separated from the higher energy levels, and so the system may be described by a qubit model,

$$H = \sum_{i=1}^n \frac{\omega_i}{2} Z_i + D_i(t) X_i + \sum_{\langle i,j \rangle} J_{ij} Y_i Y_j, \quad (3)$$

where the notation X, Y, Z has been used for the Pauli matrices.

Single qubit X, Y and Z terms can be independently controlled by applying a pulse at zero detuning with the drive envelope parameterized as

$$d_i(t) = (h_i^X(t) + ih_i^Y(t)) \exp \left(-2i\Omega \int_0^t h_i^Z(t') dt' \right). \quad (4)$$

In the frame rotating at the qubit frequencies, the effective Hamiltonian resulting from this drive is

$$H(t) = \frac{\Omega}{2} \sum_i [h_i^X(t) X_i + h_i^Y(t) Y_i + h_i^Z(t) Z_i]. \quad (5)$$

The coupling parameter J_{ij} in FF transmon devices cannot be controlled, and thus needs to be small enough compared to the detuning between connected qubits that in the absence of driving the qubits are effectively decoupled. In this case, an entangling operation can be switched on by driving one qubit at the resonant frequency of another to which it is coupled [24, 28]. To first order, the off-resonant drive generates no dynamics. However, to second order interplay between the drive and

the static coupling results in an effective *cross-resonance* entangling operation of the general form

$$H_{ij}^{\text{CR}} = \sum_{A \in \{\mathbb{1}, X, Y, Z\}} c_{ij}^{\mathbb{1}A} \mathbb{1}_i A_j + c_{ij}^{ZA} Z_i A_j. \quad (6)$$

Estimations for the values of the coefficients $\{c_{ij}^k\}$ have been extracted using high order Schrieffer-Wolff perturbation theory [27, 29] but these depend on experimental parameters that are inaccessible to end users and which can drift over time. As a result, we find it more practical to extract the coefficients experimentally in a calibration process.

III. HAMILTONIAN VERIFICATION AND CALIBRATION THROUGH TOMOGRAPHY

The level of control offered by the cross-resonance Hamiltonian (Eq. (6)) theoretically allows for the simulation of a rich array of lattice spin systems. However, it is crucial to verify that the experimental dynamics continue to satisfy criteria C1-C3 in the presence of imperfections such as cavity leakage. In particular, the cross-resonance drives should not induce any dynamics on qubits other than the control and target, and the result of applying two simultaneous cross-resonance drives on two different qubits should be the sum of the individual cross-resonance interactions (i.e., $H_{1,2,3}^{\text{eff}} = H_{1,2}^{\text{eff}} + H_{2,3}^{\text{eff}}$). Quantum process tomography (QPT) is ideally suited to the verification of these properties, since it makes no assumptions about the underlying dynamics and can thus identify unexpected terms. The experimental implementation of QPT for this purpose is presented in Sec. III A.

While QPT is rigorous, it is highly inefficient, requiring a number of expectation value measurements that is proportional to d^4 (with $d = 2^n$ the dimension of the Hilbert space) to obtain the process matrix that characterizes a given channel. It is thus unsuitable for the calibration of the Hamiltonian coefficients in Eq. (6). Instead, having verified the structure of the effective Hamiltonian, these rates can be calibrated far more efficiently using *Hamiltonian tomography* [30–32], which for this system requires only five Rabi oscillation experiments for a full characterization of the effective Hamiltonian. The Hamiltonian tomography protocol used in this work is presented in Sec. III B.

A. Quantum Process Tomography

QPT yields the full process matrix characterizing the experimental dynamics, including non-unitary contributions from decoherence. For the purposes of Hamiltonian identification, only the unitary contribution of the full quantum channel is considered, and so these effects are not taken into account. The extent to which the dynamics are faithfully represented by a unitary operator is

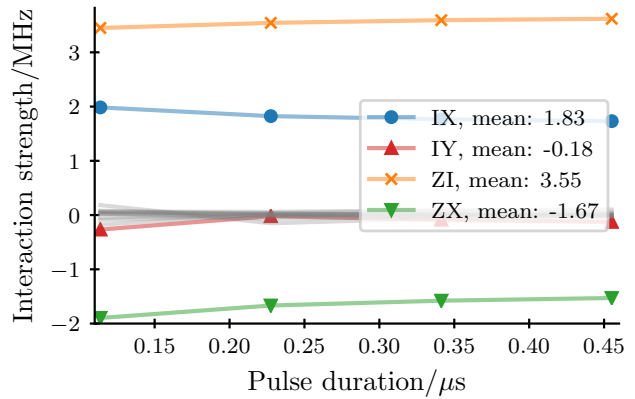


FIG. 1. Effective Hamiltonian rates extracted from full process tomography on qubits 1 and 2, implemented on the `ibmq_guadalupe` quantum device following the application of a cross-resonance drive on qubit 1 at the frequency of qubit 2 for varying pulse durations. The dominant $Z_i X_j$, $\mathbb{1}_i X_j$ and $Z_i \mathbb{1}_j$ terms are significantly stronger than any other Hamiltonian terms (shown in gray, with $\mathbb{1}_i Y_j$ shown in red as an illustration) and the rates are consistent for all drive durations as expected.

characterized by the dominant eigenvalue λ_0 of the process matrix, which is 1 for a fully unitary operator and $0 < \lambda_0 < 1$ for non-unitary operations. Since non-unitary errors cannot be directly counteracted in the scheme proposed here, this measurement represents an additional check on the viability of analogue simulation protocols.

The effective Hamiltonian may be extracted by taking the logarithm of the reconstructed unitary evolution operator. Using this method, the eigenvalues of the effective Hamiltonian are obtained only up to factors of 2π . This ambiguity can be alleviated by extracting Hamiltonian terms over a range of different pulse durations. While the cross-resonance interaction can generate interactions consisting of any coherent mixture of $Z_i X_j$ and $Z_i Y_j$ terms, for convenience here we work with interactions that are aligned along one axis only. This can be achieved by applying a drive pulse with a purely real drive envelope (i.e., $h_i^Y = 0$ in Eq. (4)), resulting in only $Z_i X_j$ interactions, along with the spurious single qubit rotations to be characterized. In practise, we find that the experimental pulse envelopes can accumulate significant phase errors. These can be eliminated by adjusting the phase of the drive envelope until no $Z_i Y_j$ interactions are observed. This calibration procedure has been performed prior to performing all of the experiments presented here.

Fig. 1 shows the observed effective Hamiltonian rates for a series of cross-resonance interactions applied on the `ibmq_guadalupe` quantum device, with the minimum factors of π needed to generate linear plots added. Factors of π rather than 2π are added since the terms that dominate the dynamics ($Z_i X_j$, $\mathbb{1}_i X_j$ and $Z_i \mathbb{1}_j$) mutually commute, meaning that there is an additional ambiguity arising from the fact that adding π to any term results in an

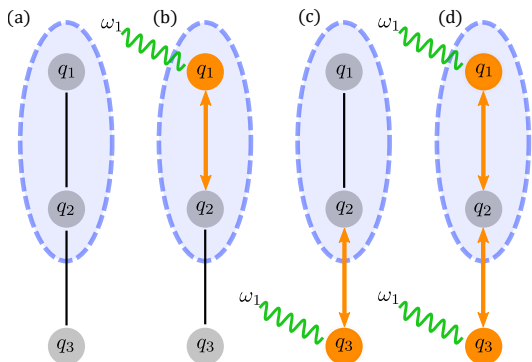


FIG. 2. Schematic diagram for the series of process tomography experiments used to verify the qualitative form of the cross-resonance effective Hamiltonian Eq. (6). In all cases, full QPT is performed on qubits 1 and 2. (a) No drives are applied (b) Qubit 1 is driven at the frequency of qubit 2 (c) Qubit 3 is driven at the frequency of qubit 2 (d) Both qubit 1 and qubit 3 are simultaneously driven at the frequency of qubit 2.

unmeasurable global phase. These largest terms correspond to the terms predicted by Eq. (6), showing that the qualitative features of the cross-resonance gate are indeed reliable for this system. Additionally, the largest eigenvalue for the process matrices generated by these experiments was approximately 0.93, showing that the dynamics are dominated by the unitary evolution. Given that the reported measurement error rates for IBM Quantum devices are on the order of 1% [28], it is reasonable to ascribe a large portion of the non-unitary errors to state preparation and measurement errors.

To verify that the effective Hamiltonian for the three qubit channel is the sum of the two qubit effective Hamiltonians (i.e., $H_{1,2,3}^{\text{eff}} = H_{1,2}^{\text{eff}} + H_{2,3}^{\text{eff}}$), we use four two-qubit QPT experiments, where the tomography is performed on qubits 1 and 2 after the application of the following different drive protocols (outlined schematically in Fig. 2):

1. No drives, leave the qubits idle for the drive duration.
2. Drive qubit 1, leave qubit 3 idle.
3. Drive qubit 3, leave qubit 1 idle.
4. Drive both qubit 1 and 3 simultaneously.

If the effective Hamiltonian generating the dynamics observed in experiment 4 is equal to the sum of Hamiltonians for the previous three experiments, then it can be concluded that the Hamiltonian for the full n -qubit system may be obtained by characterizing all qubit pairs involved in the experiment. Additionally, experiment 3 may be used to confirm that no unexpected additional terms are generated on idle qubits – that is, the dynamics observed in experiment 3 should only be single qubit X rotations. Fig. 3 summarises the experimental results

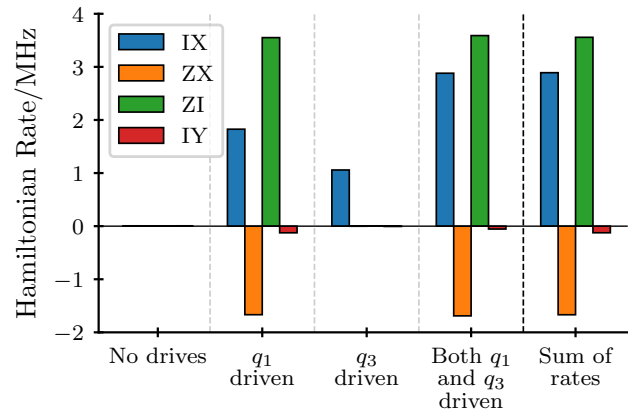
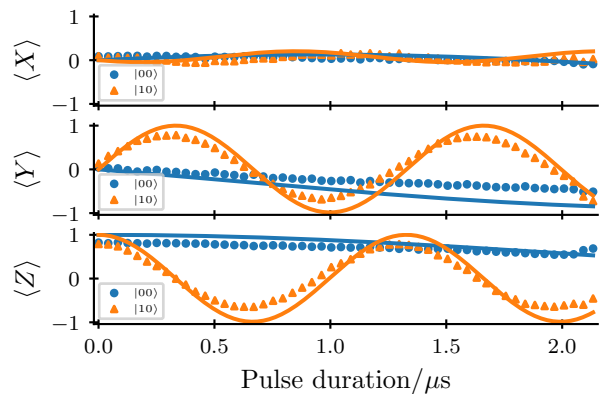


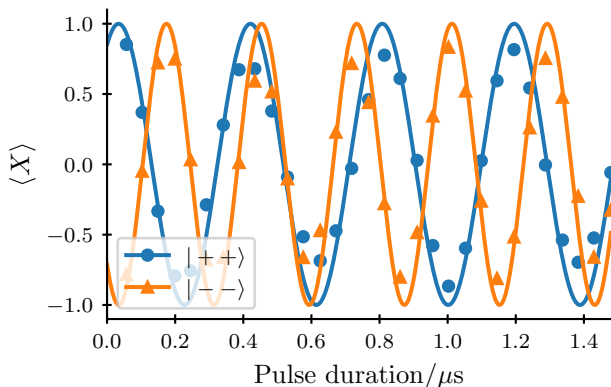
FIG. 3. Summary of Hamiltonian rates obtained from the application of experiments 1-4 explained in the main text and summarised in Fig. 2, with the tomography performed on qubits 1 and 2 (shown by the blue ellipses), implemented on the `ibmq_guadalup` quantum device. Terms with rates less than 0.2 have been dropped for clarity, with the exception of c_{1Y} , which is shown for comparison. The first four sets of bars correspond to the experimental data for the various driving setups, while the final set corresponds to the predicted values for driving qubits 1 and 3 simultaneously, obtained as the sum of the Hamiltonian rates for driving qubits 1 and 3 separately plus the idle Hamiltonian, which is approximately vanishing. This predicted set of rates is very close (within 1.5%) to the real experimental rates for the simultaneous drive with the exception of the $1_i Y_j$ rate, which is at a much lower magnitude and is therefore more susceptible to measurement error. This indicates that the simultaneous drive can indeed be modelled accurately as the sum of the individual effective Hamiltonians.

from experiments 1-4. As expected, no additional terms are observed on qubits 1 and 2 when qubit 3 is driven, regardless of whether qubit 1 is itself driven. Additionally, the predicted rates arising from adding the Hamiltonian rates for experiments 1-3 (final set of bars in Fig. 3) matches the results of experiment 4 very well, with all the rates apart from c_{1Y} (the rate of the $1_i Y_j$ term) differing by less than 0.05MHz, or less than 1.5% of the observed Hamiltonian rates. The error for c_{1Y} was slightly higher, at 0.07MHz, however this is likely due to its significantly lower relative size, making it more susceptible to fluctuations due to measurement error. This indicates that the experimental drive behaves as indicated by Eq. (6), without significant cross-talk, and that the effective Hamiltonians for smaller subsystems can be added to obtain the dynamics for larger systems.

We note that we have not investigated longer-distance coupling on the basis that we have not observed cross-talk between next-nearest neighbours, which makes longer-range couplings unlikely. Under this assumption, the characterization of a full n -qubit system can be performed using a number of experiments that is independent of n by characterizing disconnected sets of qubits in



(a)



(b)

FIG. 5. Dynamics generated by applying the cross-resonance interaction over increasing pulse durations, with a drive amplitude of $\Omega = 36$ MHz. (a) Expectation value evolution resulting from measuring qubit 2 in each Pauli basis following evolution from $|00\rangle$ (blue) and $|10\rangle$ (orange). (b) Rabi oscillations resulting from applying the cross resonance channel on the $|++\rangle$ (blue) and $|--\rangle$ (orange) initial states, measuring the first qubit. For both plots, points correspond to experimental data obtained from the `ibm_hanoi` quantum device and the solid lines correspond to numerical expectation values extracted from evolution of the cross-resonance Hamiltonian predicted by the fits to the experimental data. The amplitudes of the oscillations are slightly reduced due to measurement error. The Hamiltonian rates obtained from these fits are given in Table. I.

raphy implemented on the `ibm_hanoi` quantum device. This is to be expected given the full QPT results above. The solid lines in both Fig. 5a and Fig. 5b are generated by numerically evolving the cross-resonance Hamiltonian obtained from the fits to the experimental data. In both cases, the points are the raw experimental data. The suppression in the observed amplitudes is most likely due to measurement error since it is present at $t = 0$. The Hamiltonian rates obtained from the tomography are given in Table I. By far the largest term, at over 3MHz is the $Z_i \mathbb{1}_j$ term arising from the AC Stark shift

Hamiltonian term	Rate/MHz
$Z_i X_j$	-0.4915
$Z_i Y_j$	-0.0332
$Z_i Z_j$	0.0294
$\mathbb{1}_i X_j$	0.4168
$\mathbb{1}_i Y_j$	0.0649
$\mathbb{1}_i Z_j$	-0.0756
$Z_i \mathbb{1}_j$	3.0810

TABLE I. Cross-resonance Hamiltonian rates extracted from the `ibm_hanoi` quantum device using Hamiltonian tomography as described in the main text, with the applied drive amplitude $\Omega = 36$ MHz. The dynamics are dominated by the AC Stark shift $Z_i \mathbb{1}_j$ term, which can be eliminated by adjusting the qubit drive frequency or by applying a dynamic phase to single qubit pulses, leaving dynamics generated principally by the desired $Z_i X_j$ and $\mathbb{1}_i X_j$, the latter of which can be eliminated by the addition of a simultaneous resonant pulse on the target qubit. All other terms are significantly smaller.

on the control qubit from the off-resonant drive. This is expected to be the case based on theoretical predictions (the Stark shift term is proportional to the square of the applied drive amplitude Ω , whereas the other terms are proportional to either $J_{ij}\Omega$ or J_{ij}^2 , with $J_{ij} \ll \Omega$).

The next largest rates are the desired entangling operator $Z_i X_j$ and the spurious single qubit $\mathbb{1}_i X_j$ rotation, which for these qubits and drive parameters have equal and opposite rates with magnitudes approximately 0.5MHz. All other terms have substantially smaller magnitudes and can be neglected. In particular, the two-body $Z_i Y_j$ and $Z_i Z_j$ terms, arising from residual drive phase miscalibration and qubit-qubit self-interaction respectively, are the smallest and are more than an order of magnitude smaller than the desired $Z_i X_j$ term. These are the most problematic terms, since they cannot be eliminated using single qubit quantum control.

In order to use the cross-resonance interaction for analogue quantum simulation, it is necessary to be able to control all the Hamiltonian terms. As shown in Eq. (4), the single qubit terms can be controlled or eliminated through the addition of resonant control pulses, while the magnitude of the two-body interactions is controlled by the amplitude of the cross-resonance drive. Since changing this amplitude also changes all the other Hamiltonian rates, a strategy for implementing analogue quantum simulation in this platform would be to fix the cross-resonance amplitude, and only use single qubit control to implement the desired simulation.

A reasonable initial target would be to generate a pure Ising-type interaction (after basis change) of the form

$$H = \sum_{\langle i,j \rangle} J_{ij}^{ZX} Z_i X_j . \quad (7)$$

In order to accomplish this, single qubit control pulses can be used to cancel the remaining spurious terms. These compensation pulses must be applied at very small

amplitudes compared with those typically used for single qubit control. For comparison, the resonant amplitude for implementing a single qubit X gate on an IBM Quantum device is typically 30 MHz, approximately sixty times that needed to eliminate the spurious $\mathbb{1}_i X_j$ term. It is often assumed that low amplitude drives are unproblematic, however, in real experiments implementing such small drives can cause significant problems, which will be shown in the following section.

IV. OTHER SOURCES OF ERROR

From the above analysis, it has been demonstrated that criterion (C1) (the device must be sufficiently expressible) for the implementation of analogue quantum simulations on FF transmon qubits is indeed satisfied, and that criterion (C2) (the device must be controllable) can be satisfied as long as the small pulses necessary to cancel the spurious single qubit terms can be implemented accurately. While the fidelity of single qubit dynamics is typically assumed to be much higher than that of entangling operations [34, 35], this breaks down in the low-amplitude regime necessitated by the analogue simulation protocol proposed here.

The weakness of the effective cross-resonance interaction also means that simulations must be run for longer times than single qubit resonant dynamics to observe interesting dynamics. As an illustrative example, consider a calibrated $Z_i X_j$ drive with a strength of 0.5 MHz. In order to simulate the time dynamics of this system for a duration $J_{ZX}t = 1$ (not an especially ambitious goal considering gate-based methods implemented on IBM Quantum devices are capable of exceeding such times for many systems of interest [36, 37]) the pulses need to be applied for a duration of $2\mu\text{s}$. In principle, this is not an issue, since the reported decoherence and dephasing times for FF devices significantly exceed these times (they are typically on the order of $100\mu\text{s}$ [38]), meaning that the coherence requirement of criterion (C3) (the device should be stable) should be satisfied. Since the viability of analogue quantum simulation relies heavily upon this feature of FF transmon qubits, the reliability of these decoherence times should be verified in real experimental settings. Additionally, over such long durations, small errors can greatly reduce the fidelity of the applied dynamics, making characterization of the dynamics at low pulse amplitudes and over long times crucial for analogue quantum simulation.

A. Low Amplitude Errors

One problematic source of errors arising from the weak cross-resonance interaction is the deviation from theoretical predictions for low amplitude (Ω less than approximately 1.5MHz) resonant drives. This has significant implications for the realization of the analogue simulations

described here due to the weakness of the cross-resonance interaction compared to typical resonant control.

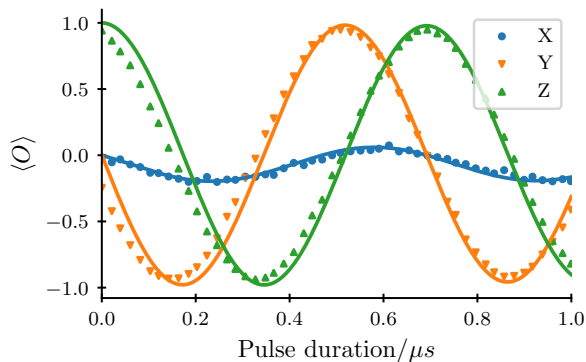
The dynamics generated by a weak resonant pulse can be investigated using single qubit quantum state tomography following the evolution of the $|0\rangle$ state over time. Given the weak nature of the pulse and the fact that any coupled qubits have frequencies which are well detuned from the drive qubit, it is reasonable to ignore spectator qubits.

Following Eq. (5) and applying pulses which are approximately constant such that h_i are approximately time-independent (with deviations from this primarily arising from the non-zero pulse ramp time), the resulting dynamics can be fit to a model Hamiltonian of the form

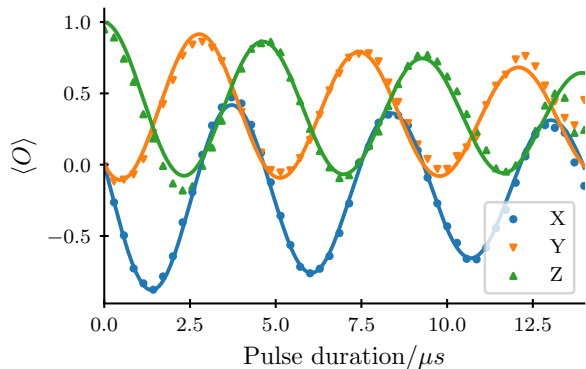
$$H = \frac{\Omega}{2} (h^X X + h^Y Y + h^Z Z) . \quad (8)$$

For the purposes of this work, the target channel is generated by the application of a purely real pulse with zero detuning such that the effective Hamiltonian is simply $\frac{1}{2}\Omega X$. By performing the state tomography experiments over an array of pulse durations, the magnitudes of the X, Y and Z terms can be extracted, allowing for the phase (resulting in spurious Y terms), detuning (resulting in spurious Z terms) and amplitude (resulting in incorrect Rabi frequencies) errors to be characterized. Since the necessary evolution times for investigating such weak fields are long enough for dephasing and decoherence effects to be observed, an additional exponential decay of the form $\exp(-t/T_2)$ was included in the dynamics, allowing for an approximation of the T_2 decay time to also be extracted. Fig. 6 shows the results of such a state tomography scheme for two low amplitudes, 0.07 MHz, corresponding to 0.0005% of the maximum drive amplitude accessible through the IBM Pulse platform and 1.50MHz, corresponding to 0.01% of the maximum drive amplitude. It should be stressed that although these amplitudes are very small when compared with typical resonant control pulses on FF qubits, it is often necessary to use such low amplitudes for cancelling the spurious terms in the cross-resonance Hamiltonian.

For both Fig. 6b and Fig. 6a, there are significant amplitude, phase and detuning errors, with the relative size of the errors being much higher for the lower drive amplitude. For Fig. 6a, the experimental Rabi frequency (obtained as $\sqrt{(h^X)^2 + (h^Y)^2}$) was observed to be 1.44MHz, corresponding to an error of 0.06MHz or 4%. The phase error (obtained by fitting h^X and h^Y to Fig. 6a and then obtaining the phase of $h^X + ih^Y$) was found to be -0.04 with the detuning error being 0.05MHz. The origin of these errors is most likely due to miscalibration: since the typical target amplitudes for implementing quantum gates are as high as possible without inducing unwanted transitions, the experimental settings for the resonant drives will be calibrated for this regime. The low amplitudes used in these experiments are far from this regime, and so moderate non-linearities in the control hardware could result in deviations between the software and the



(a)



(b)

FIG. 6. Single qubit quantum state tomography results showing $\langle X \rangle$, $\langle Y \rangle$ and $\langle Z \rangle$ expectation values over varying drive durations, with drive amplitudes of (a) 1.50 MHz and (b) 0.07 MHz, implemented on the `ibm_hanoi` quantum device. The points correspond to experimental data and the solid lines correspond to fits to Eq. (8), from which phase, detuning and amplitude errors may be extracted. For (a), the observed Rabi frequency was 1.44MHz, the observed phase error was -0.04π and the observed detuning was 0.05MHz. For (b), the observed Rabi frequency was 0.16MHz, the observed phase error was 0.65π and the observed detuning was 0.07MHz. The observed T_2 time for both (a) and (b) was $31.69\mu s$ (this was extracted from (b) and used in the plots of both (a) and (b)).

experimental realization. While these deviations are not ideal, and could cause problems for an experimental simulation in which precise parameters are required, in principle the errors can be counteracted by adjusting the amplitude, phase and frequency of the applied pulse.

For Fig. 6b, the experimental errors are much higher, with the observed Rabi frequency being 0.16 MHz, corresponding to an error of 0.09 MHz or 129% of the theoretical drive. The phase error was also significantly higher, at approximately 0.65π , while the observed detuning was 0.07 MHz. The latter two errors, although higher than Fig. 6a, should also be able to be corrected in the same way. The amplitude error, however, cannot be fixed in software, as it likely arises from the finite resolution

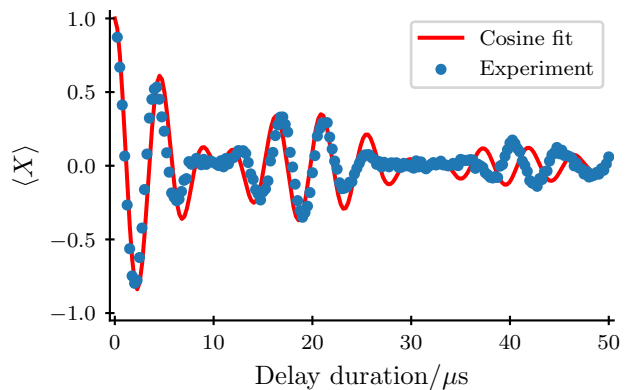


FIG. 7. Plot of spurious dynamics observed on the `ibm_hanoi` quantum device in the absence of driving as a function of delay time, with the points corresponding to the experimental data and the red line corresponding to a least squares best fit to Eq. (9). The qubit is initialised in the $|+\rangle$ X eigenstate, left idle for varying durations and measured in the X basis. The same dynamics were not observed for the same experiment performed in the Z basis, indicating the presence of a spurious Z field. Given the structure of the observed interaction, the most likely explanation is that it is caused by coupling to a two level system defect in the superconducting material.

of the arbitrary waveform generators (AWGs). AWGs with more than the required resolution can be built using commercially-available components [39]. Thus, while this is a limiting factor preventing the implementation of analogue quantum simulations on currently available devices, it should not represent an insurmountable challenge for such an implementation in the near future.

B. Spurious Dynamics in the Undriven System

A second consequence of the weak cross-resonance interaction is that the simulations need to be performed for longer times than for resonant single qubit dynamics (on the order of approximately $10\mu s$). Both the reported T_2 and bare T_2^* dephasing times for the IBM Quantum devices should be long enough for this to be achieved [38]. However, experimentally, additional spurious terms may be observed which significantly impact the behaviour of FF transmon systems over this time period. This is illustrated when one attempts to measure the dephasing of the system experimentally. The dephasing of a quantum system can be experimentally measured by initializing in the $|+\rangle$ state, waiting for varying durations, and then measuring in the X eigenbasis. In a system with dephasing error, the expectation value should exhibit an exponential decay over the characteristic T_2^* time. In the absence of any driving or spurious fields, there should not be any oscillatory behaviour. This is not necessarily the case experimentally. Fig. 7 shows the results of performing such an experiment on the `ibm_hanoi` quan-

tum device, with the results being dominated by strong oscillations. This effect is not symmetric for all axes: performing the same experiment in the Z eigenbasis results in no such oscillations, implying that the effect arises due to a spurious Z field.

The oscillations in Fig. 7 may be fit to a function of the form

$$f(t) = (c_0 \cos(f_0 t) + c_1 \cos(f_1 t)) e^{-t/T_2^*}, \quad (9)$$

with five fit parameters $\{c_0, c_1, f_0, f_1, T_2^*\}$. The results of such a fit for qubit 16 in the `ibm_hanoi` quantum device are given as the red line in Fig. 7. For this fit, the optimal frequencies were obtained as $f_0 = 0.18$ MHz and $f_1 = 0.24$ MHz, with weight coefficients $c_0 = 0.48$ and $c_1 = 0.51$. These coefficients do not reproduce the behaviour observed when measuring other qubits or when measuring the same qubit on different days and thus should be considered to be specific to this qubit at this particular time. As expected, the T_2^* time was found to be significantly shorter than the T_2 time reported by IBM, at $20.2\mu\text{s}$ as opposed to $209.6\mu\text{s}$ for this qubit. This may still be long enough to offer some advantage for analogue quantum simulation.

Since there are two observed frequencies in the oscillations, the observed dynamics cannot be explained by a simple frequency misalignment. While it is difficult to identify the source of these errors with any certainty given the limited experimental access available to end users, the form of the dynamics is consistent with coupling between the qubit and a mesoscopic environment. Such an environment could be provided by the presence of parasitic two-level systems (TLSs) [40, 41] arising from structural defects in the superconducting material. In the experiment presented in Fig. 7, coupling to a single TLS defect would induce the observed dynamics. The presence of TLSs in superconducting qubits is well known to be a significant source of decoherence [42], and could be generated through background radioactivity or cosmic rays [43]. It is likely that the TLS coupling also induces significant decoherence, reducing the observed T_2^* time. Eliminating this coupling could therefore significantly increase the decoherence times, allowing for longer analogue simulation times to be reached and extending the utility of such protocols. The nature of the spurious dynamics varies significantly over time. Fig. 8(a) shows 100 repetitions of the dephasing test outlined above, obtained on a different day to the data presented in Fig. 7 but for the same qubit and device. The blue lines show individual evolution for a characteristic subset of 20 experiments, with the blue shaded region corresponding to the upper and lower bounds of the obtained results. These data also show similar oscillatory behaviour, but cannot be well reproduced by fits to Eq. (9). This can be explained by the qubit coupling to multiple TLS defects rather than a single one as in Fig. 7. Moreover, the oscillations fluctuate significantly over the time scale during which the experiments were performed (approximately six hours), indicating that the cause of the oscillatory

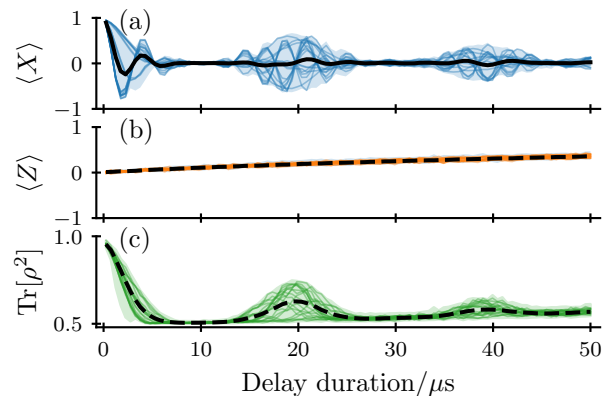


FIG. 8. Single qubit time dynamics and purity measurements corresponding to experiments initialized in $|+\rangle$ and measured in all three Pauli bases following different delay times, with the experiments implemented on the `ibm_hanoi` quantum device. The data were obtained from the same qubit as Fig. 7, but on a different day. (a) Time evolution of $\langle X \rangle$ expectation values, with the black line corresponding to the mean evolution, the blue lines corresponding to experimental evolution and the shaded region bounding the highest and lowest points observed. (b) Time evolution of $\langle Z \rangle$ expectation values, with the black line corresponding to the mean evolution, the orange lines corresponding to experimental evolution and the shaded region bounding the highest and lowest points observed. (c) Purity measurements for the delay experiments. While a multi-frequency classical field together with T_2 dephasing could explain the results of (a) and (b), the revivals in the purity at approximately $20\mu\text{s}$ and $40\mu\text{s}$ in (c) cannot be explained by classical noise sources.

behaviour changes substantially on this time scale. Performing the same experiment, but measuring in the Z basis (Fig. 8(b)) yields no oscillations for any of the 100 experimental repetitions, providing further evidence that the dynamics are induced by an effective Z field. The increase in the $\langle Z \rangle$ expectation value over time arises from the decay of the initial state $|+\rangle$ to a linear combination of $|+\rangle$ and $|-\rangle$ over time due to dephasing.

The black line in Fig. 8(a) shows the average behaviour across all experimental runs, with the limiting behaviour trending towards an exponential decay. Performing the delay experiment on different qubits on different days does not always result in oscillations, but can also result in decay behaviour similar to this mean behaviour. If the variation in the oscillatory dynamics can be explained by coupling to a mesoscopic TLS environment in which the number of defects is not constant over time, then the time-average behaviour of this system is likely to be qualitatively similar to coupling between a qubit and a bulk environment of defects. This decay behaviour could therefore be plausibly explained by coupling to a macroscopic environment of TLS defects.

The identification of the source of the oscillations with coupling to a low-dimensional environment is further reinforced by Fig. 8(c), which shows the purity of the sin-

gle qubit state as a function of delay time for the same experiments as Figs. 8(a) and (b). The purity measurements show a significant revival at approximately $20\mu\text{s}$ and a smaller revival at approximately $40\mu\text{s}$. Such revivals cannot be explained by classical sources of noise (such as, for example, magnetic fields induced by nearby power lines) and are indicative of coherent coupling between the qubit and some other quantum object. This is further evidence in support of the identification of the spurious dynamics with coupling to a low-dimensional environment consisting of TLS defects.

There is therefore strong evidence that the observed dynamics are due to a coherent coupling process between the qubit and some other quantum object. Based on the form of the oscillations and the fact that TLSs have been identified as a major source of decoherence in other superconducting platforms, it is reasonable to identify this quantum object with TLS defects. However, this cannot be rigorously verified (nor, indeed, disproven) using the level of experimental access available to end users. The spurious oscillating terms, regardless of their origin, are a significant barrier to the implementation of analogue quantum simulation on FF transmon qubits and thus the experimental investigation of their origin is of crucial importance if such a goal is to be achieved.

V. CONCLUSION AND OUTLOOK

Quantum simulation is one of the flagship applications of quantum devices. Current digital devices satisfy almost all of the criteria necessary for the realization of such simulations, but gate errors continue to pose significant problems for digital simulation methods such as Trotterization.

Analogue quantum simulation is an alternative route towards realizing Hamiltonian simulation. We experimentally evaluate fixed-frequency transmon qubits against three criteria which must be satisfied in order to realise analogue quantum simulation experimentally: (C1) expressibility, (C2) controllability and (C3) stability.

Our results indicate that superconducting fixed-frequency devices are a flexible and highly controllable analogue simulation platform, and we demonstrate that the Hamiltonian of the system can be measured quickly and with high confidence.

We find that the weakness of the cross-resonance interaction causes significant issues. At the low amplitudes required to counteract the spurious single qubit terms arising from the cross-resonance interaction, significant phase, amplitude and detuning errors cause problematic deviations from the ideal resonant drive. At moderate drive amplitudes these can be addressed on currently available devices by calibrating the drive pulses, but for very low amplitudes the limited resolution of the arbitrary waveform generators (AWGs) precludes such calibration protocols from being realized. This issue could be

easily addressed using high resolution AWGs, and thus is not a significant limiting factor for the implementation of analogue quantum simulations on FF transmon qubits. Criteria (C1) (the system Hamiltonian must be expressible enough to permit simulation of systems of interest) and (C2) (the system must be controllable such that individual Hamiltonian terms can be switched on and off independently) may then be satisfied with only modest improvements to current FF transmon implementations.

Alternatively, the floor on the implementable drive pulse amplitudes could be interpreted as a minimum disorder term for analogue simulations. For the example drives here, the minimum disorder would correspond to approximately one third of the $Z_i X_j$ interaction strength, although the precise value varies from qubit to qubit.

A more problematic issue is diagnosed through the presence of dynamical evolution on qubits which are initialized in an X eigenstate and left without additional drive pulse. We attribute the observed dynamics to coupling to two level system defects, which is known to be a major source of decoherence in other superconducting platforms. Since the spurious dynamics fluctuate over time, any protocol designed to eliminate the interaction would need to account for this fluctuation in order to ensure that criterion (C3) (the system must remain stable over the duration of the simulation) is satisfied.

Since rigorous verification and full characterization of the TLS interaction are not possible with the level of experimental access available to end users, a crucial route for further investigation lies in the application of spectroscopic techniques reported in other superconducting quantum platforms for the full characterization of this effect [44] and in the development of an effective method to eliminate these interactions. While the focus of this work is on the evaluation of analogue quantum simulations on FF qubits, TLS coupling has been identified as a key source of decoherence in superconducting platforms [42], and so a focus on addressing this problem could have wide-reaching implications beyond this application.

In summary, FF transmon qubits have great potential as a platform for analogue quantum simulation due to their ability to implement a wide array of physically interesting Hamiltonians. The primary limiting factors preventing the implementation of such simulations on current devices are the limited resolution of the control pulses and spurious coupling to two level system defects. The former can be straightforwardly eliminated with either modest hardware improvements or incorporation of the limitations into the simulations, while the latter requires further experimental work identify, characterize and eliminate the coupling. Overcoming these limitations will allow for the realization of the potential of FF transmon qubits for analogue quantum simulation.

VI. ACKNOWLEDGMENTS

We are grateful to Johannes Knolle, Kiran Khosla and Francesco Petiziol for providing stimulating discussions. This work is supported by Samsung GRP grant, the UK Hub in Quantum Computing and Simulation, part of the UK National Quantum Technologies Programme with funding from UKRI EPSRC grant EP/T001062/1 and the QuantERA ERA-NET Co-fund in Quantum Technologies implemented within the European Union's Horizon 2020 Programme. This research is part of the Munich Quantum Valley, which is supported by the

Bavarian state government with funds from the Hightech Agenda Bayern Plus. S.G. is supported by a studentship in the Quantum Systems Engineering Skills and Training Hub at Imperial College London funded by EPSRC (EP/P510257/1). D.M. acknowledges funding from ERC Advanced Grant QUENOCOBA under the EU Horizon 2020 program (Grant Agreement No. 742102). A.S. was supported by a research fellowship from the The Royal Commission for the Exhibition of 1851. We acknowledge the use of IBM Quantum services for this work. The views expressed are those of the authors, and do not reflect the official policy or position of IBM or the IBM Quantum team.

-
- [1] F. Arute, K. Arya, R. Babbush, D. Bacon, J. C. Bardin, R. Barends, R. Biswas, S. Boixo, F. G. Brandao, D. A. Buell, *et al.*, Quantum supremacy using a programmable superconducting processor, *Nature* **574**, 505 (2019).
- [2] J. Preskill, Quantum computing in the NISQ era and beyond, *Quantum* **2**, 79 (2018).
- [3] I. M. Georgescu, S. Ashhab, and F. Nori, Quantum simulation, *Rev. Mod. Phys.* **86**, 153 (2014).
- [4] J. I. Cirac and P. Zoller, Goals and opportunities in quantum simulation, *Nat. Phys.* **8**, 264 (2012).
- [5] A. Blais, S. M. Girvin, and W. D. Oliver, Quantum information processing and quantum optics with circuit quantum electrodynamics, *Nat. Phys.* **16**, 247 (2020).
- [6] R. Blatt and C. F. Roos, Quantum simulations with trapped ions, *Nat. Phys.* **8**, 277 (2012).
- [7] A. Browaeys and T. Lahaye, Many-body physics with individually controlled Rydberg atoms, *Nat. Phys.* **16**, 132 (2020).
- [8] S. Lloyd, Universal quantum simulators, *Science* **273**, 1073 (1996).
- [9] H. F. Trotter, On the product of semi-groups of operators, *Proceedings of the American Mathematical Society* **10**, 545 (1959).
- [10] B. P. Lanyon, C. Hempel, D. Nigg, M. Müller, R. Geritsma, F. Zähringer, P. Schindler, J. T. Barreiro, M. Rambach, G. Kirchmair, *et al.*, Universal digital quantum simulation with trapped ions, *Science* **334**, 57 (2011).
- [11] R. Barends, A. Shabani, L. Lamata, J. Kelly, A. Mezzacapo, U. L. Heras, R. Babbush, A. G. Fowler, B. Campbell, Y. Chen, *et al.*, Digitized adiabatic quantum computing with a superconducting circuit, *Nature* **534**, 222 (2016).
- [12] X. Peng, J. Du, and D. Suter, Quantum phase transition of ground-state entanglement in a heisenberg spin chain simulated in an NMR quantum computer, *Phys. Rev. A* **71**, 012307 (2005).
- [13] M. Endres, M. Cheneau, T. Fukuhara, C. Weitenberg, P. Schauss, C. Gross, L. Mazza, M. C. Banuls, L. Pollet, I. Bloch, *et al.*, Observation of correlated particle-hole pairs and string order in low-dimensional Mott insulators, *Science* **334**, 200 (2011).
- [14] D. Greif, T. Uehlinger, G. Jotzu, L. Tarruell, and T. Esslinger, Short-range quantum magnetism of ultracold fermions in an optical lattice, *Science* **340**, 1307 (2013).
- [15] M. Greiner, O. Mandel, T. Esslinger, T. W. Hänsch, and I. Bloch, Quantum phase transition from a superfluid to a Mott insulator in a gas of ultracold atoms, *Nature* **415**, 39 (2002).
- [16] A. A. Houck, H. E. Türeci, and J. Koch, On-chip quantum simulation with superconducting circuits, *Nat. Phys.* **8**, 292 (2012).
- [17] M. J. Hartmann, Quantum simulation with interacting photons, *J. Opt.* **18**, 104005 (2016).
- [18] S. A. Wilkinson and M. J. Hartmann, Superconducting quantum many-body circuits for quantum simulation and computing, *Appl. Phys. Lett.* **116**, 230501 (2020).
- [19] M. J. Hartmann, F. G. Brandao, and M. B. Plenio, Quantum many-body phenomena in coupled cavity arrays, *Laser Photonics Rev.* **2**, 527 (2008).
- [20] D. P. DiVincenzo, The physical implementation of quantum computation, *Fortschr. Phys.* **48**, 771 (2000).
- [21] M. S. ANIS, Abby-Mitchell, H. Abraham, AduOffei, R. Agarwal, G. Agliardi, M. Aharoni, V. Ajith, I. Y. Akhalwaya, G. Aleksandrowicz, *et al.*, Qiskit: An open-source framework for quantum computing (2021).
- [22] P. Krantz, M. Kjaergaard, F. Yan, T. P. Orlando, S. Gustavsson, and W. D. Oliver, A quantum engineer's guide to superconducting qubits, *Appl. Phys. Rev.* **6**, 021318 (2019).
- [23] D. Malz and A. Smith, Topological two-dimensional Floquet lattice on a single superconducting qubit, *Phys. Rev. Lett.* **126**, 163602 (2021).
- [24] C. Rigetti and M. Devoret, Fully microwave-tunable universal gates in superconducting qubits with linear couplings and fixed transition frequencies, *Phys. Rev. B* **81**, 134507 (2010).
- [25] J. M. Chow, A. D. Córcoles, J. M. Gambetta, C. Rigetti, B. R. Johnson, J. A. Smolin, J. R. Rozen, G. A. Keefe, M. B. Rothwell, M. B. Ketchen, *et al.*, Simple all-microwave entangling gate for fixed-frequency superconducting qubits, *Phys. Rev. Lett.* **107**, 080502 (2011).
- [26] N. Pancotti, G. Giudice, J. I. Cirac, J. P. Garrahan, and M. C. Banuls, Quantum East model: Localization, non-thermal eigenstates, and slow dynamics, *Phys. Rev. X* **10**, 021051 (2020).
- [27] M. Malekakhlagh, E. Magesan, and D. C. McKay, First-principles analysis of cross-resonance gate operation, *Phys. Rev. A* **102**, 042605 (2020).

- [28] S. Sheldon, E. Magesan, J. M. Chow, and J. M. Gambetta, Procedure for systematically tuning up cross-talk in the cross-resonance gate, *Phys. Rev. A* **93**, 060302 (2016).
- [29] V. Tripathi, M. Khezri, and A. N. Korotkov, Operation and intrinsic error budget of a two-qubit cross-resonance gate, *Phys. Rev. A* **100**, 012301 (2019).
- [30] S.-T. Wang, D.-L. Deng, and L.-M. Duan, Hamiltonian tomography for quantum many-body systems with arbitrary couplings, *New J. Phys.* **17**, 093017 (2015).
- [31] Z. Li, L. Zou, and T. H. Hsieh, Hamiltonian tomography via quantum quench, *Phys. Rev. Lett.* **124**, 160502 (2020).
- [32] R. Ma, C. Owens, A. LaChapelle, D. I. Schuster, and J. Simon, Hamiltonian tomography of photonic lattices, *Phys. Rev. A* **95**, 062120 (2017).
- [33] M. S. ANIS, Abby-Mitchell, H. Abraham, AduOf-
fei, R. Agarwal, G. Agliardi, M. Aharoni, V. Ajith,
I. Y. Akhalwaya, G. Aleksandrowicz, *et al.*, Qiskit
experiments, available at [github.com/qiskit/qiskit-
experiments](https://github.com/qiskit/qiskit-experiments).
- [34] A. Smith, M. Kim, F. Pollmann, and J. Knolle, Simulating quantum many-body dynamics on a current digital quantum computer, *npj Quantum Inf.* **5**, 1 (2019).
- [35] J. Vovrosh, K. E. Khosla, S. Greenaway, C. Self, M. S. Kim, and J. Knolle, Simple mitigation of global depolarizing errors in quantum simulations, *Phys. Rev. E* **104**, 035309 (2021).
- [36] J. Vovrosh and J. Knolle, Confinement and entanglement dynamics on a digital quantum computer, *Sci. Rep.* **11**, 1 (2021).
- [37] M. Kapil, B. K. Behera, and P. K. Panigrahi, Quantum simulation of Klein Gordon equation and observation of klein paradox in IBM quantum computer, arXiv preprint arXiv:1807.00521 (2018).
- [38] D. Koch, B. Martin, S. Patel, L. Wessing, and P. M. Alsing, Demonstrating NISQ era challenges in algorithm design on IBM's 20 qubit quantum computer, *AIP Adv.* **10**, 095101 (2020).
- [39] J. Lin, F.-T. Liang, Y. Xu, L.-H. Sun, C. Guo, S.-K. Liao, and C.-Z. Peng, Scalable and customizable arbitrary waveform generator for superconducting quantum computing, *AIP Adv.* **9**, 115309 (2019).
- [40] S. de Graaf, L. Faoro, L. Ioffe, S. Mahashabde, J. Burnett, T. Lindström, S. Kubatkin, A. Danilov, and A. Y. Tzalenchuk, Two-level systems in superconducting quantum devices due to trapped quasiparticles, *Sci. Adv.* **6**, eabc5055 (2020).
- [41] J. Lisenfeld, G. J. Grabovskij, C. Müller, J. H. Cole, G. Weiss, and A. V. Ustinov, Observation of directly interacting coherent two-level systems in an amorphous material, *Nat. Commun.* **6**, 1 (2015).
- [42] M. Müller, K. Hammerer, Y. Zhou, C. F. Roos, and P. Zoller, Simulating open quantum systems: From many-body interactions to stabilizer pumping, *New Journal of Physics* **13**, 085007 (2011).
- [43] M. McEwen, L. Faoro, K. Arya, A. Dunsworth, T. Huang, S. Kim, B. Burkett, A. Fowler, F. Arute, J. C. Bardin, *et al.*, Resolving catastrophic error bursts from cosmic rays in large arrays of superconducting qubits, *Nat. Phys.* **18**, 107 (2022).
- [44] Y. Dong, Y. Li, W. Zheng, Y. Zhang, Z. Ma, X. Tan, and Y. Yu, Measurement of quasiparticle diffusion in a superconducting transmon qubit, *Appl. Sci.* **12**, 8461 (2022).